Turkish Journal of Chemistry

http://journals.tubitak.gov.tr/chem/

Research Article

Turk J Chem
(2023) 47: 436-447

doi:10.55730/1300-0527.3550

H_2(g) production from dimethylamine borane by Cu^0/WO_3 NPs catalyst

Doaa AL-HAMEEDAWI, Seda KARABOĞA*, İzzet Amour MORKAN
Department of Chemistry, Bolu Abant İzzet Baysal University, Bolu, Turkey

Received: 03.11.2022 • **Accepted/Published Online:** 21.02.2023 • **Final Version:** 28.04.2023

Abstract: Cu^0 NPs supported on tungsten (VI) oxide (WO_3) were in situ generated from the reduction of Cu^{2+} ions during dehydrogenation of dimethylamine borane (DMAB). The Cu^0/WO_3 NPs displayed tangible catalytic activity in H_2 (g) releasing reaction and they were identified by using advanced techniques. Cu^0/WO_3 NPs were found as active catalyst providing one equiv. H_2(g) per mole of DMAB. The results from TEM images display the formation of Cu^0 NPs with an average particle size of 4.6 ± 1.0 nm on the surface of WO_3. Moreover, Cu^0/WO_3 NPs with various metal loadings were prepared and tested as catalyst in dehydrogenation reaction to find the optimum metal loading on WO_3 support. The highest H_2 generation rate was achieved for 4.0% wt. Cu^0/WO_3 catalyst with TOF value of 39 h^{-1} in the reaction conditions. Additionally, effect of various catalyst concentration and temperature is discussed on the reaction kinetics for reaction catalyzed by Cu^0/WO_3 NPs.

Key words: H_2 (g) generation, dimethylamine borane, Cu^0 nanoparticles, tungsten(VI) oxide, heterogeneous catalysis

1. Introduction

In the next century, global innovation is necessary for sustainable energy due to peripheral damage by burning fossil fuels [1]. In this regard, the development of renewable energy sources is considered urgent to facilitate the transition from fossil fuel. [2]. Hydrogen is a clean, safe, and sustainable energy carrier that can be used to overcome this problem. [3]. However, the problem of finding safe hydrogen storage materials is the main issue in using H_2 for mobile and stationary fuel cell applications [4,5]. Borane nitrogen compounds have attracted more attention recently due to their high hydrogen storage capacity and stability [6–7]. Dimethylamine borane (DMAB), one of the B-N adducts, could be used as a solid hydrogen storage material [8–9]. More importantly, $(CH_3)_2NHBH_3$) is stable and low-cost for regeneration, which could release hydrogen gas with yields up to precisely 3.0 equiv. per mole of DMAB by either through hydrolysis [10,11] or 1.0 equiv. per mole of DMAB from dehydrogenation with an appropriate catalyst under ambient conditions Eq. (1) [12].

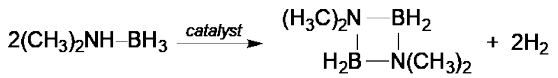

(1)

Transition metals could be used as a catalyst in H_2 (g) releasing reactions of borane adducts [13,14]. So far, homogeneous [10,15–16] and heterogeneous metal nanoparticles [17–18] have been trialed for dehydrogenation of DMAB. Among these metal nanoparticles, most of them were noble metals such as ruthenium [19–20], rhodium [21], and palladium [22]. They are more expensive than nonnoble metals. However, some of the nonnoble metals are suitable as a catalyst in H_2 releasing reactions such as copper, nickel [23,24]. Cu^0 NPs have attracted a lot of interest because copper is abundant on the earth and relatively inexpensive among these metals, and it has been used for various purposes in versatile applications and research [25]. The main problem of the Cu^0 NPs is related with the agglomeration of them during the catalytic reaction. The agglomeration of Cu^0 NPs lead to the composition of the metal bulk, which causes a fast losing to catalytic activity as expected. In this case, it is necessary to find convenient supporting supplies with huge surface area to prevent the aggregation of transition metal NPs [26]. WO_3 can be used as a proper support for metal NPs and prevents the formation of bulk metal [27]. So far, WO_3 has been approved as an effective catalyst for various reactions such as hydrolysis of ammonia borane [28], dehydrogenation of 2-butanol [29], oxidation of ethanol, and methanol [30,31]. In this report, Cu^0 NPs were stabilized by WO_3 powder due to reducible nature of WO_3 supporting material. WO_3 can facilitate transfer of electrons under reaction conditions and this status causes surplus charge on the surface. The reducible property of WO_3 improves interaction between the metal and

* Correspondence: tanyildizi_s@ibu.edu.tr

oxide support which is directly related with the catalytic performance of the catalyst. [32]. This advantage makes it a unique supporting material for the metal nanoparticles in several catalytic reactions. Herein, WO_3 supported Cu^0 NPs prepared by impregnation of Cu^{2+} ions on powder supporting material in toluene solution. The active catalyst called Cu^0/WO_3 NPs was tested as a catalyst in dehydrogenation of DMAB at 60 ± 0.5 °C. The isolated catalyst (Cu^0/WO_3 NPs) was identified by modern analytical techniques such as XRD, XPS, UV-Vis, TEM. The results of the experiments and analysis reveal that Cu^0 NPs are an active catalyst and they provide (39 h^{-1}) initial TOF in dehydrogenation reaction of DMAB at 60 ± 0.5 °C. Additionally, the report encloses the evaluation of kinetic studies of the catalytic reaction of DMAB.

2. Experimental

2.1 Materials

Tungsten trioxide (WO_3, 99.99%) was purchased from Nanografi. Toluene, copper bis(2-ethylhexanoate), and dimethylamine borane (97%) were bought from Sigma Aldrich. Toluene used as a solvent in this study was purified before performing the catalytic experiments. All glassware was cleaned with ethanol and dried at 120 °C.

2.2. Instrumentation

The same instruments have been utilized as one given our previous work, except for TEM and UV-Vis analysis [31]. While the TEM images of the Cu^0/WO_3 NPs were obtained from Hitachi HT-7700 operating at 120 kV, UV-Vis spectra of initial copper precursor Cu(II) 2-ethylhexanoate) and final catalyst Cu^0 NPs were taken by HITACHI U-2900 UV/VIS spectrophotometer.

2.3. Determination of the most effective Cu loading for Cu^0/WO_3 NPs

Different copper loaded samples (1.0%–6.0% wt.) were prepared in order to determine the most effective Cu loading for Cu^0/WO_3 NPs. They were trialed in H_2 (g) releasing from DMAB at 60 ± 0.5 °C. The highest H_2 generation rate was obtained for the catalyst sample of 4% wt. Cu. Consequently, the catalyst sample with 4.0% wt. Cu loaded was utilized for further catalytic reactions.

2.4. Recyclability test of Cu^0/WO_3 NPs catalyst

The catalytic performance of Cu^0/WO_3 NPs in subsequent runs of the reaction was tested. A typical reaction was started by preparing a suspension containing 100 mg Cu^{2+}/WO_3 (4.0% wt. Cu) and DMAB (60.11 mg, 100 mM) at 60.0 ± 0.5 °C. The procedure was repeated for the further run of the catalytic reaction, and performance of the catalyst was evaluated with determining turnover frequency.

2.5. Kinetic parameters of the reaction catalyzed by Cu^0/WO_3 NPs

Dehydrogenation reactions were repeated with 100 mg Cu^0/WO_3 (4.0% wt.) and a steady concentration of DMAB (100mM, 60.11 mg DMAB) in 10 mL toluene solution at various temperatures in order to get the activation parameters of the reaction.

2.6. Preparation and catalytic performance of Cu^0/WO_3 NPs

Catalytic reactions were carried out under inert gas atmosphere after vacuuming and purging of all glassware with nitrogen to remove any residue of oxygen and water. To prepare a stock solution, 153.02 mg copper bis(2-ethylhexanoate) was dissolved in 25.0 mL of toluene. For the preparation of the precatalyst, 3.75 mL (17.49 mM) of stock solution was transferred to a flask containing 100 mg of WO_3 dissolved in 3.25 mL of fresh toluene. Next, DMAB dispersed in 3.0 mL toluene was added to the reaction medium. The slurry with a volume of 10.0 mL was stirred for an hour for impregnation of copper (II) ions on the surface of WO_3. After an hour, DMAB was transferred to reaction medium by a gas-tight syringe. The reaction was followed until no more gas evolution.

3. Results and discussion

3.1. In situ preparation of Cu^0 NPs supported on WO_3

The reduction of Cu^{2+} ions on the surface of WO_3 supporting material lead to active catalyst called Cu^0/WO_3 NPs. Cu^0/WO_3 NPs were tested as a catalyst in H_2(g) generation from DMAB after the catalytic activity of bare Cu^{2+} ions were determined without using any stabilizer in dehydrogenation reaction. The comparison of H_2 evolution from DMAB with bare Cu^{2+}, bare WO_3 and Cu^{2+}/WO_3 NPs can be seen in Figure 1. The same amount of Cu concentration was used in both experiments to compare each other. Although hydrogen evolution starts within a few minutes, bare Cu^0 NPs have an initial 11.44 h^{-1} TOF value, lose their catalytic activity during the reaction course due to the aggregation of Cu^0 NPs in the medium. The observation of bulk copper metal at the bottom of the reaction tube is also an evidence of the agglomeration of Cu^0 NPs. The comparison of bare and WO_3-supported Cu^0 NPs indicates that adding 2-ethylhexanoate as only stabilizer in the

reaction medium could not prevent the agglomeration of Cu^0 NPs. On the other hand, Cu^0/WO_3 NPs exhibit important catalytic performance with 39 h^{-1} TOF value in the same catalytic reaction. It can be concluded that WO_3 supporting material increases the catalytic activity of Cu^0 NPs more than three times due to the large surface area. The complete H_2 (g) production from DMAB was seen when the WO_3-supported Cu^0 NPs were used as an active catalyst. Therefore, WO_3 was preferred as a stabilizer for Cu^0 NPs. The comparison of bare Cu^0 NPs, bare WO_3, and WO_3-supported Cu^0 NPs in Figure 1 indicates that WO_3 could prevent the aggregation of Cu^0 NPs during the catalytic reaction.

The experiment was performed starting with 6.65 mM of copper(II) 2-ethylhexaonate, and 100 mg of WO_3 in 10 mL of toluene. After addition of DMAB into the reaction medium, the color of the solution changes to dark brown. The traceable change in color of the solution allows following the reaction by UV-Vis. Figure 2 shows the UV-Vis spectrum of Cu^0/WO_3 NPs solution before and after transfer of DMAB into the reaction medium. UV-Vis spectrum of the beginning solution containing Cu^{2+} ions indicates a sharp absorption band at 290 nm and a broad band at around 651 nm. While the sharp absorption band at 290 nm is attributed to LMCT the other band at 651 nm shows the d-d transition of the copper salt used as a precursor in this study [33]. The new spectrum obtained after the reaction was completed demonstrates that the bands disappeared and a new band at 289 nm was observed. This new band that appeared at 289 nm shows typical Mie scattering for Cu^0 NPs, which implies the formation of Cu^0 during the catalytic reaction [34].

The isolated Cu^0/WO_3 NPs were identified by modern analytical techniques. Figure 3 displays the powder X-ray diffraction patterns of bare WO_3 and WO_3-supported Cu^0 NPs. Both samples show the same diffraction peaks that belong to WO_3 (ICDD Card No: 43-1035), which approves that: (i) the traceable peak would be attributed to Cu has not been seen, probably due to lower metal loading and (ii) the lattice and crystallinity of WO_3 are not affected by reduction of Cu^{2+} ions to Cu^0 on the surface of powder WO_3 supporting material. Moreover, the positions of diffraction peaks of WO_3 maintain their initial positions after Cu loading on the surface of WO_3 sample. As a result, it can be expressed that Cu loading does not alter the infrastructure of support.

TEM images of Cu^0/WO_3 NPs samples with 4.0% Cu loaded are shown in Figure 4. In more details, TEM images with different magnification explain that Cu^0 NPs are well-dispersed on the surface of WO_3. The particle size histogram was constructed by counting more than 100 nontouching particles, and the mean diameter of Cu^0 NPs was found as (4.6 ± 1.0) nm.

XPS analysis offers important insights for the chemical state information of copper in the catalyst sample from the surface of Cu^0/WO_3. The survey analysis of Cu^0/WO_3 NPs sample in Figure 5 displays the copper element with the framework elements of WO_3. High-resolution spectrum of Cu 2p bands indicates that two prominent peaks at 932.8 and 952.7 eV belong to metallic Cu $2p_{3/2}$ and $Cu2p_{1/2}$, respectively [35,36]. XPS analysis is evidence of reduction of Cu^{2+} ions used as a precursor and existence of metallic Cu as a Cu^0 form in the catalyst sample.

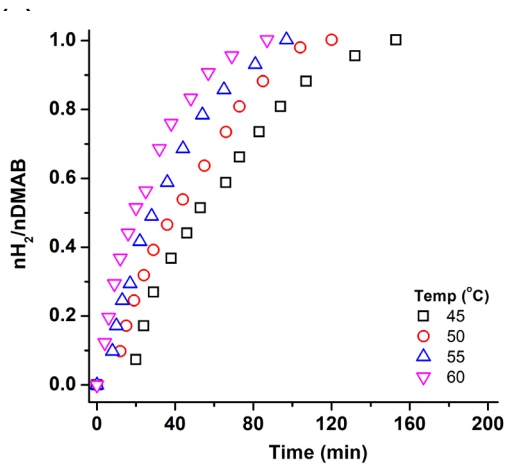

Figure 1. Plots of mol H_2/mol DMAB versus time for H_2 production reaction catalyzed by bare Cu^0 NPs (red circle), WO_3 supported Cu^0 NPs (blue triangle) and bare WO_3 (black square) at 60.0 ± 0.5 °C.

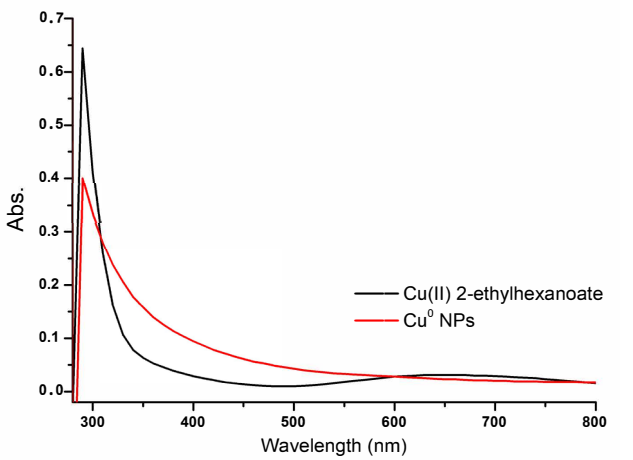

Figure 2. UV-Vis spectra of Cu precursor solution before and after addition of 100 mM DMAB 60.0 ± 0.5 °C.

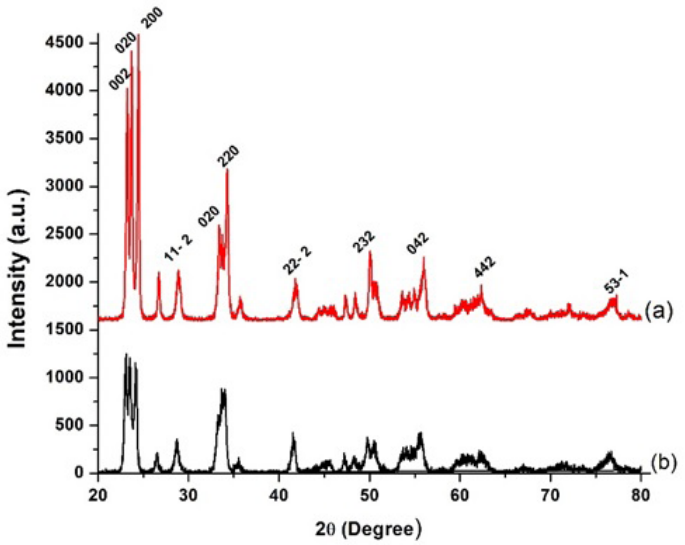

Figure 3. Powder p-XRD patterns of a) unloaded WO_3 nanopowder (red line), b) WO_3 supported Cu0 NPs (Cu^0/WO_3, 4.0% Cu wt.).

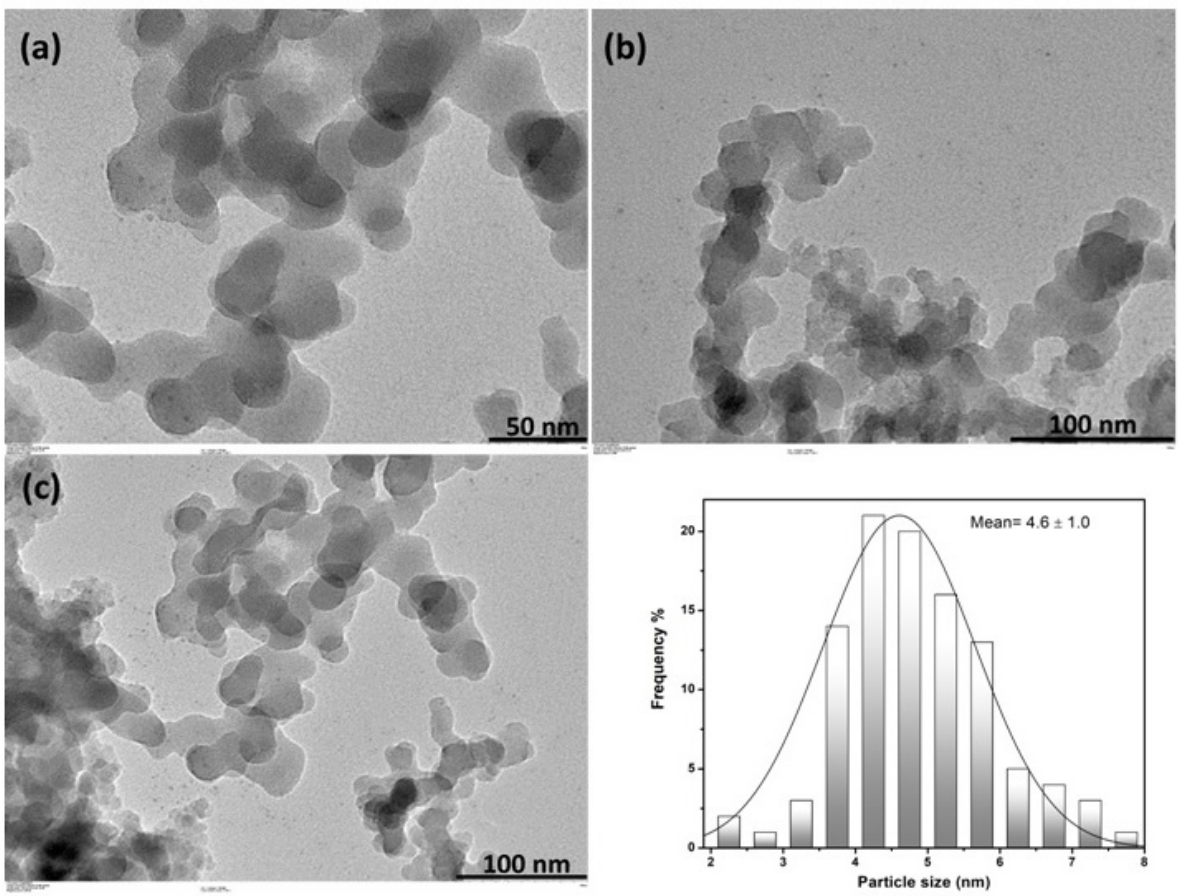

Figure 4. (a,b,c) TEM images of Cu^0/WO_3 with Cu 4.0 % loading after dehydrogenation of DMAB in different magnifications 50, 100 nm d) The histogram of Cu^0 NPs.

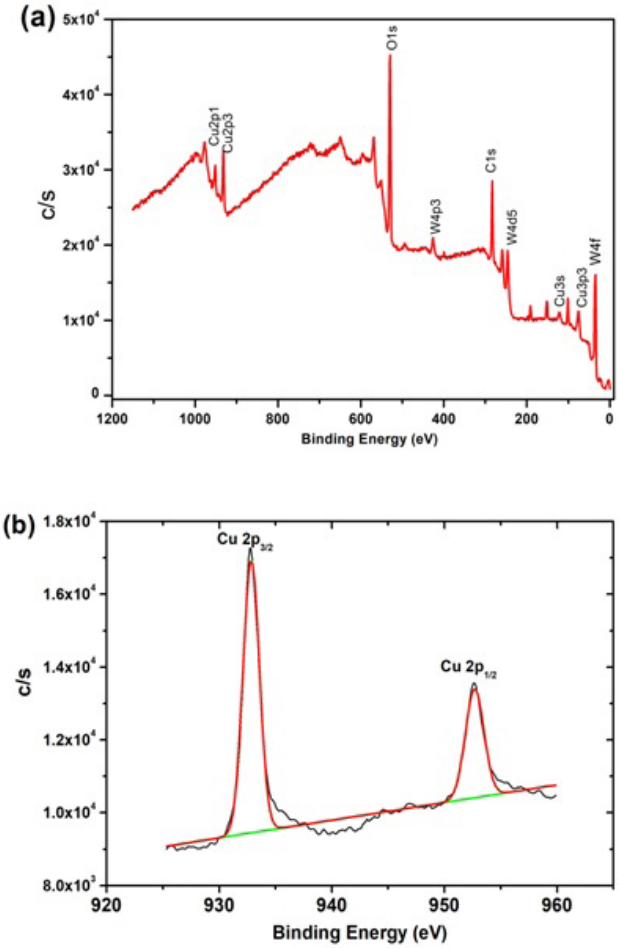

Figure 5. (a) (XPS) survey scan of Cu^0/WO_3 catalyst sample (Cu 4.0% wt.), (b) Detailed analysis of Cu 2p bands.

3.2. Catalytic performance of Cu^0/WO_3 NPs

Firstly, the catalytic activity of bare WO_3 sample was tested in H_2 generation from DMAB starting with 100 mg of WO_3 in 10.0 mL of toluene. The reaction was followed for at least one hour. It is obviously clear that WO_3 is catalytically inert in its bare form for the dehydrogenation reaction. Next, Cu-loaded WO_3 samples with different percentages of Cu were prepared and trialed in dehydrogenation of DMAB. Figure 6a shows the H_2(g) evolution graph from DMAB catalyzed by Cu^0/WO_3 NPs with different Cu loading in the range 2%–8% wt. Cu. H_2 evolution starts within a few minutes after transfer of DMAB substrate into reaction mixture and continue until 1.0 equiv gas evolved from the catalytic reaction. The sample with 4.0% wt. Cu loaded found as the most active catalyst in H_2 (g) production from DMAB. The H_2 generation rate of the catalyst was calculated as 39 h^{-1} for Cu^0/WO_3 NPs with 4.0% wt. Cu. The relationship between the catalytic activity of the catalyst and copper loadings in the sample can be seen in Figure 6b. A volcano-shaped variation was seen as the copper loading increased most probably due to pile aggregation of Cu^0 NPs on the surface of supporting material during the reaction. The further copper loadings lead to a decrease in surface area of the supporting material and failure to reach active sites of the catalyst. Therefore, the Cu^0/WO_3 samples with a ratio of 4.0% wt. Cu were used as the optimum ratio for all further experiments in this work. In order to determine the effect of catalyst concentration, the rate of the reaction was determined from each graph. As shown in Figure 6c, a straight line with a slope of 0.94 indicates that the catalytic reaction is a first-order reaction with respect to concentration of copper.

Similar experiments were performed to determine the substrate effect on the rate of dehydrogenation reaction of DMAB while keeping the catalyst concentration constant at 6.65 mM Cu (Figure 7a). It can be clearly seen from the slope

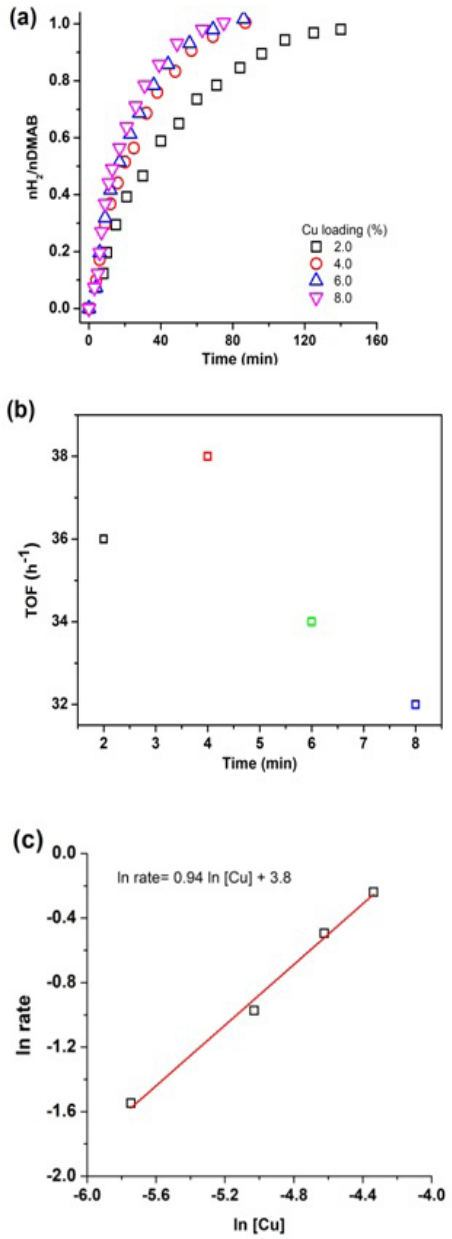

Figure 6. (a) Plots of mol H_2/mol DMAB versus time for hydrogen generation from dehydrogenation of 100 mM DMAB in different copper loadings (2%, 4%, 6%, 8% wt. Cu), (b) TOF values versus Cu loadings of catalyst Cu^0/WO_3, c) Logarithmic plot of rate versus metal concentration.

of line in Figure 7b that hydrogen generation rate from the catalytic dehydrogenation of DMAB is actually independent of DMAB concentration. Thus, dehydrogenation of DMAB catalyzed by Cu^0/WO_3 NPs is approximately zero order with respect to the substrate concentration. Thus, the rate law of dehydrogenation reaction can be given as Eq. (2):

$$\text{Rate} = k^{app}[Cu]^a[DMAB]^b, \quad (2)$$

where a and b were found as 0.94 and 0.28, respectively.

The dehydrogenation experiments were also repeated to determine the activation parameters of the reaction. The catalytic performance of WO_3 supported Cu0 NPs at different temperatures can be seen in Figure 8a. The rate constant for each plot was calculated from the experimental data and utilized to draw the Arrhenius and Eyring plots [37,38]. The slope of the Arrhenius (Figure 8b) and Eyring plots (Figure 8c) gave the activation energy and entropy of the catalytic reactions as E_a =37 ± 2 kJ mol^{-1}, $\Delta H^{\#}$=35 ± 2 kJmol^{-1} and $\Delta S^{\#}$=−148 ± 2 JK^{-1}mol^{-1}, respectively, which are comparable to that previously reported in the literature [39]. Table indicates the catalyst used in dehydrogenation of DMAB with TOF values and some reaction parameters.

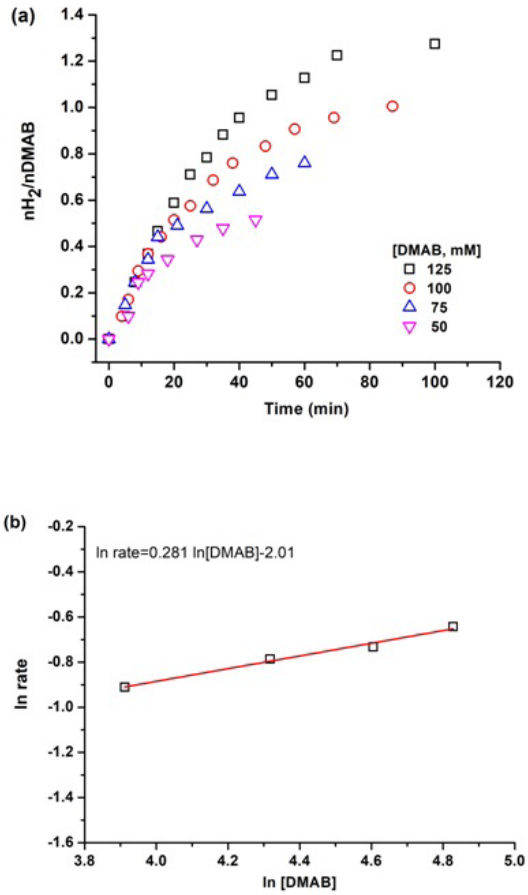

Figure 7. a) The plot of hydrogen generation graph with different substrate concentration in the range of 50–125 mM while keeping the catalyst concentration 6.65 mM for each experiment, b) ln rate vs ln DMAB graph.

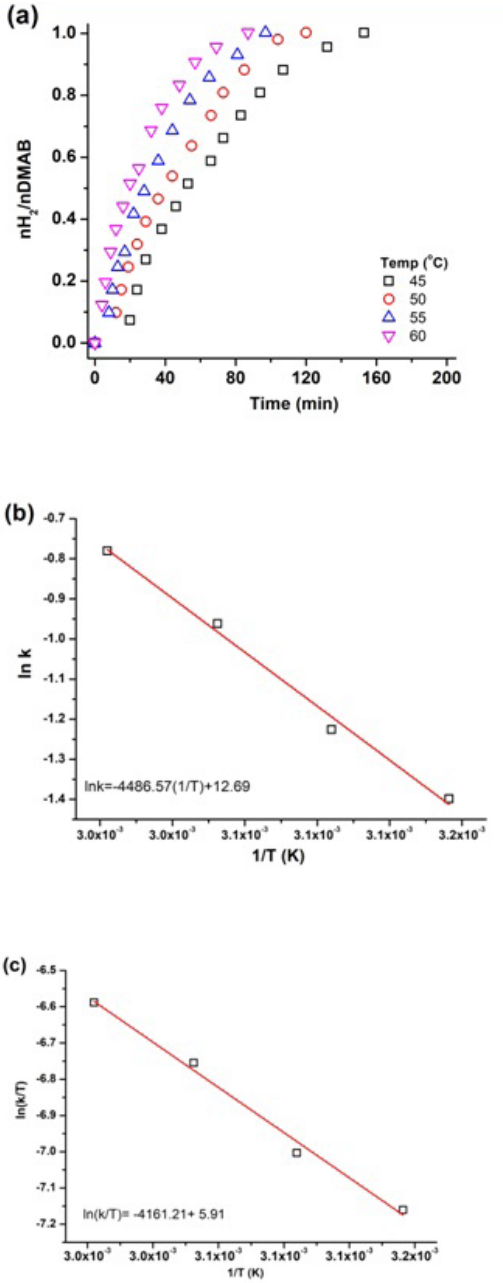

Figure 8. a) H_2 evolution graph of 100 mM DMAB catalyzed by Cu^0/WO_3 NPs (%4.0 Cu wt) at various temperatures (45–60 °C), b) Arrhenius, and c) Eyring plot.

Table. Comparison of the TOF values and some reaction parameters of the catalysts used in H2 generation from DMAB.

					Equiv. H_2				
Entry	**Precatalyst /catalyst**	**Solvent**	**T (°C)**	**Time (h)**	**per mole of DMAB**	**Particle size(nm)**	**TOF (h^1)**	**E_a (kJ/mol)**	**Ref.**
1	$[Ru(H)(PMe_3)(N(C_2H_4P^iPr_2)_2]$	THF	25	28	1.0	-	1.5	-	[40]
2	$[Rh(1,5\text{-cod})(\mu\text{-Cl})]_2$	Toluene	25	8	1.0	-	12.4	-	[10]
3	Cp_2Ti	Toluene	20	4	1.0	-	12.3	-	[41]
4	$[Ir(1,5\text{-cod})(\mu\text{-Cl})]_2$	Toluene	25	136	0.95	-	0.7	-	[10]
5	$Rh(0)/[Noct_4]Cl$	THF	25	6	0.9	2.0	8.2	-	[42]
6	$RhCl_3$	Toluene	25	23	0.9	-	7.9	-	[10]
7	$[RhCl(PHCy_2)_3]$	Toluene	25	19	1.0	-	2.6	-	[47]
8	Rh(0) Nanoclusters	Toluene	25	2.5	1.0	1.9	60	34	[22]
9	Pd(0)/MOF	Toluene	25	6	1.0	4.3	75	173.5	[43]
10	Pt(0)NPs/AA	THF	25	0.6	1.0	3.3	15	64	[44]
11	Pt(0)/TBA	THF	25	1	1.0	3.9	31	46.7	[45]
12	$[PtH(I^tBu)(I^tBu)]$	THF	25	-	1.0	-	-	-	[46]
13	Pt(0)/DPA@GO	THF	25	1	1.0	3.6	35	42	[47]
14	OAm-stabilized Ru(0)NPs	Toluene	25	1.5	1.0	1.8	137	29	[48]
15	Ru(0)APTS	THF	25	2	1.0	1.7	55	61	[49]
16	OAm-stabilized Cu(0) NPs	Toluene	50	1.3	1.0	3.5	158	19	[23]
17	$Cu(0)/CeO_2$	Toluene	60	0.6	1.0	3.1	40	76	[46]
18	$Pd(0)/Al_2O_3$	Toluene	25	1.3	1.0	7.1	73	36	[29]
19	$Ru(0)/CeO_2$	Toluene	60	1	1.0	1.8	812	62	[25]
20	Cu^0/WO_3	Toluene	60	1.5	1.0	4.6	39	37	This Study

In order to explain the catalytic performance of Cu^0/WO_3 NPs in subsequent runs, recyclability tests were also executed. The system was preserved without any alterations after first run of the catalytic dehydrogenation and the same amount of dimethylamine borane was added into the medium. H_2 (g) generation was followed for the following runs of the catalytic reaction. It was seen in Figure 9, Cu^0/WO_3 NPs catalyst remains catalytically active in H_2(g) generation from DMAB more than three cycles of the dehydrogenation reactions. The decrease in catalytic activity of the Cu^0/WO_3 NPs attributed to the fact that addition of more DMAB in further runs causes the agglomeration of Cu^0 NPs on the surface of the supporting material. The other reason for the decrement of catalytic activity of the reaction is related to the accumulation of the side product of the DMAB.

The catalytic lifetime of WO_3 supported Cu^0 NPs in H_2 releasing from DMAB was determined by measuring the total turnover number (TTON). Lifetime of the catalyst was performed starting with 0.0654 mmol Cu in 10.0 mL toluene solution including 100 mg WO_3 sample and 250.0 mM DMAB at 60.0 ± 0.5 °C (Figure 10). TTON of the catalyst was measured by adding more DMAB after each complete conversion. The reaction was followed until no more hydrogen evolution was observed. Initial TOF value of 30 h^{-1} was obtained for Cu^0/WO_3 NPs in lifetime experiment performed at 60.0 ± 0.5 °C. The decrease in catalytic activity within hours indicating the deactivation of the catalyst

Poisoning experiment was also carried out to test whether the catalytic dehydrogenation reaction of DMAB is homogeneous or heterogeneous. The poisoning test for Cu^0/WO_3 NPs catalyst was performed with CS_2 (0.2 eqiv. per mole of catalyst used). After evolution of 50% H_2 from the reaction, 0.2 eqiv. CS_2 was transferred to reaction flask via gas tight syringe. Hydrogen evolution was suddenly ceased and no more H_2 evolved from the reaction. It was clearly seen in Figure 11 that Cu^0 NPs supported on surface of WO_3 act as a heterogeneous catalyst during the dehydrogenation of DMAB.

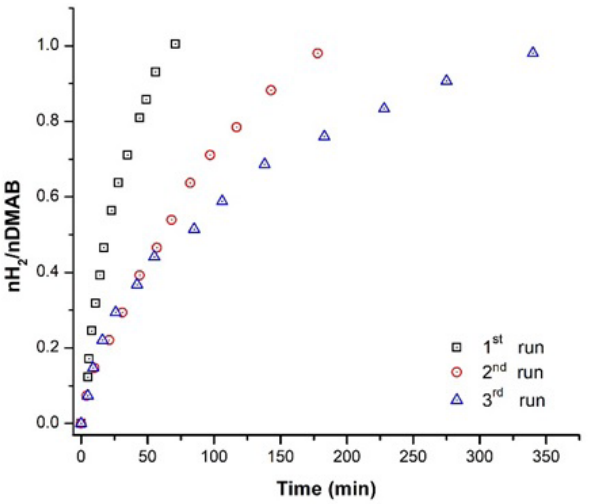

Figure 9. Dehydrogenation plots of 100 mM DMAB catalyzed by Cu^0/WO_3 NPs with 4.0% wt. Cu. in the subsequent runs.

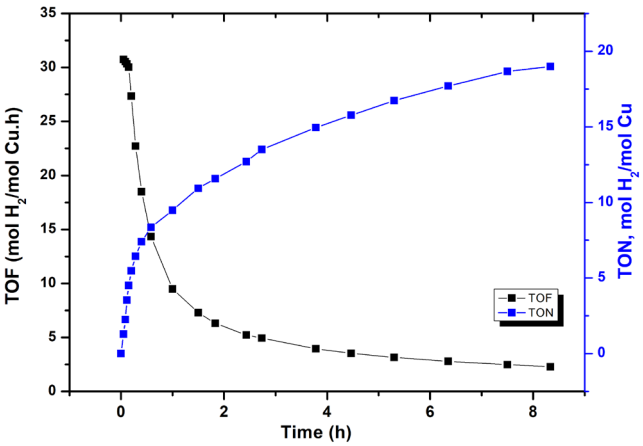

Figure 10. Catalytic lifetime of Cu^0/WO_3 NPs catalyst in dehydrogenation of DMAB using 6.54 mM Cu in 10.0 mL toluene solution including 100 mg of WO_3 sample and 250.0 mM DMAB at 60.0 ± 0.5 °C.

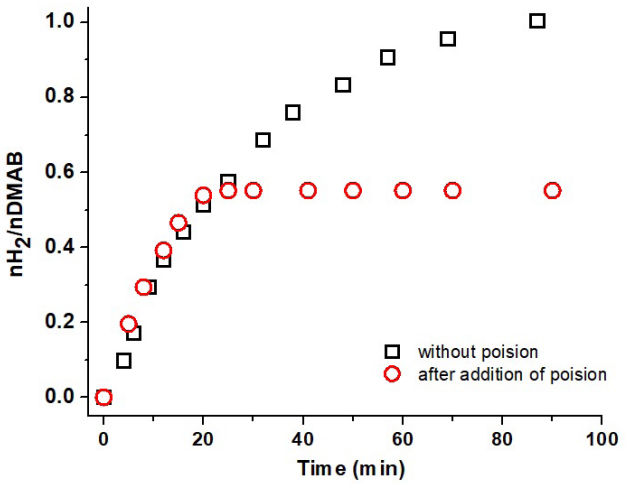

Figure 11. Plots of nH_2/nDMAB vs time for dehydrogenation of DMAB catalyzed by 4.0% wt. Cu/WO3 NPs before and after addition of 0.20 eqiv. of CS_2 at 60.0 ± 0.5 °C.

4. Conclusion

The main outputs of the study can be summarized as: Cu^0 NPs obtained from the reduction of Cu(II) ions show a catalytic activity in dehydrogenation of DMAB. However, they need a stabilizer to prevent the agglomeration during the reaction course. WO_3 was used as stabilizer for Cu^0 NPs in this study. The comparison of bare and WO_3-supported Cu^0 NPs indicates that usage of supporting material increase the catalytic activity of Cu^0 NPs more than three times in H_2 releasing reaction of DMAB at 60.0 ± 0.5 °C.

1) Isolated Cu^0/WO_3 NPs were characterized by advanced techniques (XRD, TEM, XPS, and UV-Vis spectroscopy). The results disclosed that Cu^0 NPs with a mean particle size as 4.6 ± 1.0 nm could be stabilized on surface of WO_3.

2) The order of reaction found as one was calculated from the results of kinetic studies with respect to catalyst concentration.

3) Recyclability tests clarified that Cu^0/WO_3 NPs lose their initial activity in the further catalytic cycles. The decreased in activity of the Cu^0/WO_3 catalyst for the sequent runs may be due to the aggregation of Cu^0 NPs on the surface of tungsten(VI) oxide.

4) Relatively high activity, low cost, and the simple preparation of Cu0/WO3 catalyst make the Cu^0 NPs possible nominee to be utilized as attractive catalysts in developing an efficacious H_2(g) production using DMAB as solid hydrogen storage materials.

References

1. Eberle U, Felderhoff M, Schüth F. Chemical and physical solutions for hydrogen storage.
2. Angewandte Chemie International Edition 2009; 48 (36): 6608-6630. https://doi:10.1002/anie.200806293
3. Schlapbach L, Zuttel A. Hydrogen-storage materials for mobile applications. Nature 2001; 414 (6861): 353-358. https://doi:10.1038/35104634
4. Graetz J. New approaches to hydrogen storage. Chemical Society Reviews 2009; 38 (1): 73-82. https:// doi.org/10.1039/B718842K
5. Schlapbach L, Züttel A. Hydrogen-storage materials for mobile applications. 2011; 265-270. https://doi:10.1038/35104634
6. Hwang HT, Varma A. Hydrogen storage for fuel cell vehicles. Current Opinion in Chemical Engineering 2014; (5): 42-48. https:// doi.org/10.1016/j.coche.2014.04.004
7. Demirci UB, Akdim O, Andrieux J, Hannauer J, Chamoun R, Miele P et al. Sodium borohydride hydrolysis as hydrogen generator: issues, state of the art and applicability upstream from a fuel cell. Fuel Cells 2010; 10 (3): 335-350 https://doi.org/10.1002/fuce.200800171
8. Karahan S, Zahmakıran M, Özkar S. Catalytic hydrolysis of hydrazine borane for chemical hydrogen storage: highly efficient and fast hydrogen generation system at room temperature. International Journal Hydrogen Energy 2011; (36): 4958-4966. https://10.1016/j.ijhydene.2010.12.129
9. Jaska CA, Temple K, Lough AJ, Manners I. Transition metal-catalyzed formation of boron–nitrogen bonds: catalytic dehydrocoupling of amine-borane adducts to form aminoboranes and borazines. Journal of the American Chemical Society 2003; (125): 9424-9434. https://doi.org/10.1021/ja030160l
10. Wechsler D, Cui Y, Dean D, Davis B, Jessop PG. Production of H_2 from combined endothermic and exothermic hydrogen carriers. Journal of the American Chemical Society 2008; (130): 17195-17203. https://doi.org/10.1021/ja806721s
11. Munoz-Olasagasti M, Telleria A, Perez-Miqueo J, Garralda MA, Freixa Z et al. A readily accessible ruthenium catalyst for the solvolytic dehydrogenation of amine-borane adducts. Dalton Transactions 2014, (43): 11404-11409. https://doi.org/10.1039/C4DT01216J
12. Caliskan S, Zahmakiran M, Durap F, Özkar S. Hydrogen liberation from the hydrolytic dehydrogenation of dimethylamine-borane at room temperature by using a novel ruthenium nanocatalyst. Dalton Transactions 2012; (41): 4976-4984. https://doi.org/10.1039/C2DT00042C
13. Turner J, Sverdrup G, Mann K, Maness PG, Kroposki B, Ghirardi M, Evans RJ, Blake D. et al. Renewable hydrogen production. International Journal Energy Research 2008; (32): 379-407. https://doi.org/10.1002/er.1372
14. Özkar S. Enhancement of catalytic activity by increasing surface area in heterogeneous catalysis. Applied. Surface Science 2009; (256): 1272-1277. https://doi.org/10.1016/j.apsusc.2009.10.036
15. Özkar S. Transition metal nanoparticles as catalyst in hydrogen generation from the boron based hydrogen storage materials S.L. Suib (Ed.), New and future developments in catalysis. Batteries, hydrogen storage and fuel cells, Elsevier, 2013, p. 165
16. Barin E U, Masjedi M, Ozkar S. A New Homogeneous Catalyst for the Dehydrogenation of Dimethylamine Borane Starting with Ruthenium(III) Acetylacetonate. Materials 2015; 8 (6): 3155-3167. https://doi:10.3390/ma8063155.
17. Sloan ME, Clark TJ, Manners I. Homogeneous catalytic dehydrogenation/dehydrocoupling of amine-borane adducts by the Rh(I) Wilkinson's complex analog RhCl(PHCy2)3 (Cy = cyclohexyl). Inorganic Chemistry 2009; (48): 2429-2435 https://doi: 10.1021/ic801752k
18. Zahmakiran M, Özkar S. Dimethylammonium hexanoate stabilized rhodium(0) nanoclusters identified as true heterogeneous catalysts with the highest observed activity in the dehydrogenation of dimethylamine–borane. Inorganic Chemistry 2009; (48): 8955-8964. https://doi:10.1021/ic9014306
19. Tanyildizi S, Morkan I, Özkar S. Nanotitania-supported rhodium(0) nanoparticles: superb catalyst in dehydrogenation of DMAB. Chemistry Select 2017; (2): 5751-5759. https://doi.org/10.1002/slct.201700872
20. Karaboga S, Ozkar S. Ceria supported ruthenium nanoparticles: Remarkable catalyst for H_2 evolution from dimethylamine borane. International Journal of Hydrogen. Energy 2019; 44 (48): 26296-26307. https://doi.org/10.1016/j.ijhydene.2019.08.103

21. Karatas Y, Acidereli H, Gulcan M, Sen F. A novel highly active and reusable carbon based platinum-ruthenium nanocatalyst for dimethylamine-borane dehydrogenation in water at room conditions. Scientific Reports 2020; (10): 7149. https://doi: 10.1038/s41598-020-64046-9

22. Karaboga S. Tungsten(VI) oxide supported rhodium(0) nanoparticles; highly efficient catalyst for H_2 production from dimethylamine borane. International Journal of Hydrogen. Energy. 2021; 46 (34): 17763-17775. https://doi.org/10.1016/j.ijhydene.2021.02.188

23. Karaboga S, Ozkar S. Nanoalumina supported palladium(0) nanoparticle catalyst for releasing H_2 from dimethylamine borane. Applied Surface Science. 2019; (487): 433-441. https://doi.org/10.1016/j.apsusc.2019.05.087

24. Demir H, Duman S. Monodisperse nickel nanoparticles in the solvent-free dehydrogenation of dimethylamine borane, International Journal of Hydrogen. Energy 2015; 40(32): 10063-10071. https://doi:10.1016/j.ijhydene.2015.06.093

25. Karacan Y, Karaboga S, Morkan I. Cu^0/TiO_2 nanoparticles as active catalyst for H_2 production from dimethylamine borane. ChemistrySelect 2021; (6): 7076–7081. https://doi.org/10.1002/slct.202101405

26. Yousef A, Barakat NAM, El-Newehy MH, Ahmed MM, Kim HY. Catalytic hydrolysis of ammonia borane for hydrogen generation using Cu(0) nanoparticles supported on TiO2 nanofibers. Colloids Surf. A: Physicochem. Eng. Asp. 2015; (470): 194-201.

27. Kinik FP, Nguyen TN, Mensi M, Ireland CP, Stylianou KC, Smit B. et al. Sustainable hydrogenation of nitroarenes to anilines with highly active in-situ generated copper nanoparticles. ChemCatChem 2020; (12): 2833-2839. https://doi.org/10.1002/cctc.202000150

28. Zhu QL, Xu Q. Immobilization of ultrafine metal nanoparticles to high-surface-area materials and their catalytic applications. Chem 2016; 1 (2): 220-245. https://doi.org/10.1016/j.chempr.2016.07.005

29. Akbayrak S, Tonbul Y, Özkar S. Tungsten (VI) oxide supported rhodium nanoparticles: highly active catalysts in hydrogen generation from ammonia borane. International Journal of Hydrogen Energy 2021; 46 (27): 14259-14269. https://doi:10.1016/J.IJHYDENE.2021.01.156

30. Baertsch CD, Komala KT, Chua YH, Iglesia E. Genesis of brønsted acid sites during dehydration of 2-butanol on tungsten oxide catalysts. Jornal of Catalysis 2002; 205 (1): 44-57. https://doi.org/10.1006/jcat.2001.3426

31. Rutkowska IA, Wadas A, Kulesza PJ. Mixed layered WO_3/ZrO_2 films (with and without rhodium) as active supports for PtRu nanoparticles: enhancement of oxidation of ethanol. Electrochimica Acta 2016; (210): 575-587. https://doi.org/10.1016/j.electacta.2016.05.186

32. Barczuk PJ, Tsuchiya H, Macak JM, Schmuki P, Szymanska D et al. Enhancement of the electrocatalytic oxidation of methanol at Pt/ Ru nanoparticles immobilized in different WO_3 matrices. Electrochemical and Solid-State Letters 2006; 9 (6): E13. https://doi.org/10.1149/1.2190597

33. Akbayrak S. Decomposition of formic acid using tungsten (VI) oxide supported AgPd nanoparticles. Journal of Colloid and Interface Science 2019; (538): 682-688. https://doi.10.1016/j.jcis.2018.12.074

34. A.B.P. Lever Studies in physical and theoretical chemistry. Inorganic Electronic Spectroscopy (2nd ed.), Elsevier, New York, 1984.

35. Creighton JA, Eadon DG. Ultraviolet–visible absorption spectra of the colloidal metallic elements. Journal of the Chemical Society, Faraday Transactions. 1991; (87): 3881–3891. https://doi.org/10.1039/ft9918703881

36. Miller AC, Simmons GW. Copper by XPS. Surface Science Spectra. 1993; (2): 55–60 https://doi.org/10.1116/1.1247725

37. Reddy KR, Kumar NS, Sreedhar B, Kantam ML. N-Arylation of nitrogen heterocycles with aryl halides and arylboronic acids catalyzed by cellulose supported copper(0). Journal of Molecular Catalysis A: Chemica 2006; (252): 136–141 https://doi.org/10.1016/j.molcata.2006.02.053

38. K.J. Laidler Chemical Kinetics (3rd ed.), Harper & Row Publishers, New York, 1987.

39. Eyring H. Journal of Chemical Physics1935; (3): 107-115. https://doi10.1063/1.1749604

40. Tanyildizi S, Morkan İ, Ozkar S. Ceria supported copper(0) nanoparticles as efficient and cost-effective catalyst for the dehydrogenation of dimethylamine borane. Molecular Catalysis 2017; (434): 57-68 https://doi.org/10.1016/j.mcat.2017.03.002

41. Friedrich A, Drees M, Schneider, S. Ruthenium-Catalyzed Dimethylamineborane Dehydrogenation: Stepwise Metal-Centered Dehydrocyclization. European Journal of Chemistry 2009; (15) 10339-10342. https://doi.org/10.1002/chem.200901372.

42. Clark TJ, Russell CA, Manners I. Homogeneous, Titanocene-Catalyzed Dehydrocoupling of Amine-Borane Adducts. Journal of the American Chemical Society 2006; (128): 9582-9583. https://doi.org/10.1021/ja062217k

43. Jaska CA, Manners I, Heterogeneous or homogeneous catalysis? Mechanistic studies of the rhodium-catalyzed dehydrocoupling of amine-borane and phosphine-borane adducts. Journal of American Chemical Society 2004; (126): 9776-9785 https://doi.org/10.1021/ja0478431

44. Gulcan M, Zahmakiran M, Özkar S. Palladium(0) nanoparticles supported on metal organic framework as highly active and reusable nanocatalyst in dehydrogenation of dimethylamine-borane. Applied Catalysis B: Environmental 2014; (147): 394-401. https://doi.org/10.1016/j.apcatb.2013.09.007

45. Sen F, Karatas Y, Gulcan M, Zahmakiran M. Amylamine stabilized platinum(0) nanoparticles: active and reusable nanocatalyst in the room temperature dehydrogenation of dimethylamine-borane. RSC Advances 2014; (4): 1526-1531 https://doi.org/10.1039/C3RA43701A

46. Erken E, Pamuk H, Karatepe O, Baskaya G, Sert H et al. New Pt(0) Nanoparticles as Highly Active and Reusable Catalysts in the C1–C3 Alcohol Oxidation and the Room Temperature Dehydrocoupling of Dimethylamine-Borane. Jornal of Cluster Science 2016; (27): 9-23 https://doi10.1007/s10876-015-0892-8

47. Rosello-Merino M, Lopez-Serrano J, Conejero S. Dehydrocoupling Reactions of Dimethylamine-Borane by Pt(II) Complexes: A New Mechanism Involving Deprotonation of Boronium Cations Journal of American Chemical Society 2013; (135): 10910-10913. https://doi.org/10.1021/ja404655v

48. Celik B, Baskaya G, Sert H, Karatepe O, Erken E et al. Monodisperse Pt(0)DPA@GO Nanoparticles as Highly active catalysts for Alcohol Oxidation and Dehydrogenation of DMAB. International Journal of Hydrogen Energy 2016; (41): 5661-5669 https://doi:10.1016/j.ijhydene.2016.02.061

49. Duman S, Özkar S. Oleylamine-stabilized ruthenium(0) nanoparticles catalyst in dehydrogenation of dimethylamine-borane. International Journal of Hydrogen Energy. 2013; 24 (38) 10000-10011. https://doi.org/10.1016/j.ijhydene.2013.05.119

50. Zahmakiran M, Philippot K, Özkar S, Chaudre B. Size-controllable APTS stabilized ruthenium(0) nanoparticles catalyst for the dehydrogenation of dimethylamine–borane at room temperature. Dalton Transaction 2012; (41): 590-598 https://doi. org/10.1039/C1DT11290B